







Determination of Elastic Moduli for the Geotechnical Site Characterization Using Compressional and Shear Seismic Refraction Tomography at the Proposed Site for Baba Gur-Gur University, Northeastern Kirkuk, Iraq

Ali A. Mohammed ¹, Mahmood A. Al-Mufarji ^{2*} , Ahmed J. Al-Heety ³ , Burkan S. Othman ⁴ ,
Kamal Abdelrahman ⁵ 

^{1,4} Department of Applied Geology, College of Science, Kirkuk University, Kirkuk, Iraq.

² College of Agriculture Hawija, Kirkuk University, Kirkuk, Iraq.

³ Department of Seismic Data Processing, Oil Exploration Company, Baghdad, Iraq.

⁵ Department of Geology & Geophysics, College of Science, King Saud University, Riyadh 11451, Saudi Arabia.

Article information

Received: 16- Jan -2024

Revised: 20- Feb -2024

Accepted: 14- Apr -2024

Available online: 01- Jan – 2025

Keywords:

Seismic refraction tomography
Shear wave refraction
Site characterization
Geotechnics
MASW

Correspondence:

Name: Mahmood A. Al- Mufarji

Email:

drmahmoud@uokirkuk.edu.iq





ABSTRACT

Seismic refraction tomography is carried out at a proposed site for the University of Baba Gur-Gur, Kirkuk, Iraq. Four parallel compressional and shear-wave refraction profiles are accomplished to evaluate the dynamic and elastic moduli of the underlying soil and rocks by analyzing the compressional wave (Vp) and shear wave (Vs) velocities. The Vp and Vs are obtained using two refraction tomography (P and SH) acquisitions along each line. In addition, based on these seismic wave velocities and field density values, empirical and theoretical equations are used to evaluate the dynamic and elastic moduli. The results of velocity models agree with available borehole and outcrop information and show the transition from unconsolidated sediment (topsoil) at the surface to consolidated sedimentary rocks at depth. The results indicate that the study area has four layers with fairly velocity increasing with depth. The first layer with Vp (300-310 m/s) and Vs (110 -115 m/s) predominantly consists of topsoil and forms overburden (competent and sometimes loose soil) and has a thickness (<1 m). The second layer has Vp (830-870 m/s), and Vs (310- 325 m/s) with a thickness range from (3 to 4) m. This layer is suggested to be clayey siltstone belonging to the Mukdadiya Formation. The third layer represented by relatively high Vp (1560-1580 m/s) and Vs (675-685 m/s) with a thickness range from (3 to 7 m) is suggested to be relatively denser clayey siltstone. The bedrock represented by the fourth layer with Vp > 2400 m/s and Vs >1100 m/s is considered the sandstone of the Mukdadiya Formation. According to the information provided, the 3rd and 4th layers are appropriate for the engineering project. The resulting geotechnical properties in the area can be used for the preliminary foundation design of any engineering construction.

DOI: [10.33899/earth.2024.146087.1221](https://doi.org/10.33899/earth.2024.146087.1221), ©Authors, 2025, College of Science, University of Mosul.

This is an open-access article under the CC BY 4.0 license (<http://creativecommons.org/licenses/by/4.0/>) .

حساب معاملات المرونة للتقييم الجيوتقني الموقعي باستخدام طريقة التصوير الزلزالي المقطعي الانكساري الطولي والقصي في الموقع المقترح لجامعة بابا كركر، شمال شرقي كركوك، العراق

علي أياد محمد¹، محمود عبد الله المفرجي^{2*} , أحمد جدوع الهيتي³ , بركان سعيد عثمان⁴ , كمال عبد الرحمن⁵ .
^{1,4} قسم الجيولوجيا التطبيقية، كلية العلوم، جامعة كركوك، كركوك، العراق.
² كلية الزراعة/الحويجة، جامعة كركوك، كركوك، العراق.
³ قسم معالجة البيانات الزلزالية/شركة الاستكشافات النفطية، وزارة النفط، بغداد، العراق.
⁵ قسم الجيولوجيا والجيوفيزياء، كلية العلوم، جامعة الملك سعود، الرياض 11451، المملكة العربية السعودية.

ملخص	معلومات الارشفة
تم إجراء التصوير المقطعي الزلزالي الانكساري في الموقع المقترح لإنشاء جامعة بابا كركر في كركوك. تم تنفيذ أربعة خطوط متوازية للمسح الانكساري (بالموجات الطولية) ومثلها للموجات القصية من أجل تحديد الخواص الديناميكية ومعامل المرونة للتربة والصخور من خلال تحليل السرعات الطولية (Vp) والقصية (Vs). لقد تم الحصول على Vs و Vp باستخدام طريقتي التصوير المقطعي الانكساري (SH و P) لكل خط مسح زلزالي. بالإضافة إلى ذلك، واستناداً إلى سرعات الموجات الزلزالية وقيم الكثافة المقاسة مختبرياً وتجريبياً، تم استخدام علاقات تجريبية ونظرية لتقييم المعاملات الديناميكية والمرونة. تتفق نتائج نماذج السرعة مع معلومات الابار والمكاشف الصخرية المتاحة، والتي تظهر الانتقال من الرواسب غير المتصلبة (التربة السطحية) إلى الصخور الرسوبية المتصلبة مع العمق. اشارت النتائج إلى أن منطقة الدراسة تتألف من أربع طبقات تزداد السرعة فيها مع العمق. تتكون الطبقة الأولى ذات Vp (300-310 م/ث) و Vs (110-115 م/ث) في الغالب من تربة سطحية، ويبلغ سمكها (> 1 م)، الطبقة الثانية Vp (830-870 م/ث) و Vs (310-325 م/ث) وبسماكة تتراوح من 3 إلى 4 م. ويقترح أن تكون هذه الطبقة عبارة عن حجر غريني طيني ينتمي إلى تكوين مقادادية. الطبقة الثالثة ممثلة بـ Vp (1560-1580 م/ث) و Vs (675-685 م/ث) بسمك يتراوح من 3 إلى 7 م. يقترح أن تكون أكثر كثافة نسبياً من حجر الغرين الطيني. ويعتبر صخر الأساس المتمثل بالطبقة الرابعة $V_p > 2400 \text{ m/s}$ و $V_s > 1100 \text{ m/s}$ هي صخور الحجر الرملي لتكوين مقادادية. وبحسب المعلومات المقدمة، فإن الطبقتين الثالثة والرابعة مناسبتان للمشاريع الهندسية الكبيرة. يمكن استخدام الخصائص الجيوتقنية الناتجة في المنطقة لتصميم الأساس الأولي لأي بناء هندسي مستقبلي.	<p>تاريخ الاستلام: 16- يناير -2024</p> <p>تاريخ المراجعة: 20- فبراير -2024</p> <p>تاريخ القبول: 14- ابريل -2024</p> <p>تاريخ النشر الإلكتروني: 01- يناير -2025</p> <p>الكلمات المفتاحية:</p> <p>التصوير الزلزالي الانكساري</p> <p>التصوير الزلزالي الانكساري القصي</p> <p>التوصيف الموقعي</p> <p>الجيوتقنية</p> <p>التحليل متعدد القنوات للموجات السطحية</p> <p>المراسلة:</p> <p>الاسم: محمود عبد الله المفرجي</p> <p>Email: drmahmoud@uokirkuk.edu.iq</p>

DOI: [10.33899/earth.2024.146087.1221](https://doi.org/10.33899/earth.2024.146087.1221), ©Authors, 2025, College of Science, University of Mosul.
 This is an open access article under the CC BY 4.0 license (<http://creativecommons.org/licenses/by/4.0/>).

Introduction

Assessing the cost of losses caused by building collapse and failure to infrastructures, human lives, and the environment may be challenging. Most typically, this collapse might occur from inadequate soil/rock characterization to establish the competency geomaterials limitations of the near-surface geology before a civil structure is built. The most typical technique for soil/rock characterizations is occupying excavations, borehole drillings, cores, and lab studies. The outcomes derived from these techniques are spatially limited and localized to the examined site (Das and Basudhar, 2009), and their findings may provide difficulties or impossibilities, as

well as uncertainties, in terms of generalizing them to larger areas (Mohamed *et al.*, 2013). Since the subsurface consists of various materials, the findings of a point test conducted at one location on a site may not apply to other areas of the site (Miller *et al.*, 2018). Nevertheless, depending only on typical interpretations derived from geotechnical techniques, such as boreholes, would provide insufficient soil and rock information (Cardarelli *et al.*, 2014). Numerous investigations have demonstrated that engineering decisions based solely on construction methods have a failure rate of approximately 75% (Fang *et al.*, 2019). Consequently, a thorough comprehension of the shallow geology related to the particular project is crucial in determining the optimal land utilization in various regions. As a result, it is necessary to compare the outcomes of these methods with those of other significant geophysical methods to analyze the subsurface soil/rock conditions accurately and obtain more reliable and sufficient data at a particular site (Shimobe and Spagnoli, 2020).

A geotechnical geophysics survey involves using non-destructive geophysical methods on the earth's surface to obtain reliable details about the properties and variations of the subsurface between present boreholes. This survey provides valuable geotechnical data over larger areas and allows engineers to reduce the number of required boreholes, as drilling can be expensive or impractical in specific locations (Hunt, 2005; Ehlers *et al.*, 2008). The application of near-surface geophysical techniques has been discovered to deliver highly reliable, rapid, and cost-effective approaches to the classification of geological properties, in particular at the earlier beginning of the construction of significant infrastructure projects (Sitharam *et al.*, 2008; Azwin *et al.*, 2013; Pegah and Liu, 2016). Several shallow geophysical methods employed during the site investigation include Multi-channel Analysis of Surface Waves (MASW), seismic refraction tomography (SRT), Electrical Resistivity Tomography (ERT), and Ground Penetrating Radar (GPR) method, among other techniques (Mohamed *et al.*, 2013; Gardi *et al.*, 2015; Al-Heety and Shanshal, 2016; 2022; Gardi *et al.*, 2018; Al-Saigh, and Al-Heety, 2018; Al-Nuaiemy *et al.*, 2018; Al-Heety *et al.*, 2021; Baban *et al.*, 2022; Shazly *et al.*, 2023; Ali, 2023). The SRT and MASW methods are “considered” highly effective surface non-invasive seismic geophysical methods. These methods are commonly employed in geotechnical geophysics surveys to evaluate the nature of soil and rock for civil and geotechnical engineering goals. Several studies have highlighted the success rate of these improvements (e.g., Al-Saigh and Al-Heety, 2014; Foti *et al.*, 2011).

Several studies have demonstrated the use of geotechnical and geophysical analyses to deliver foundation evaluation concerns corresponding to the conditions of the underlying soil or rock (e.g., Ozcep and Ozcep, 2011; Donohue *et al.*, 2011; Butchibabu *et al.*, 2023) were granted valuable results. The method and equipment requests for refraction surveying are specified in the ASTM standard D5777-18, 2018. The refraction processes detailed here follow a methodology similar to that outlined in ASTM D5777 for compressional waves. In the case of shear wave (SH-refraction), polarized S-waves are used, which are released from horizontal seismic sources and received via horizontal component geophones (Hunter *et al.*, 2022). The traditional methods for interpreting seismic P- and SH-wave refraction data involve a simplified model of the subsurface, which is composed of a limited number of strata with a constant velocity. Seismic refraction tomographic (SRT) methods, on the other hand, are specifically developed to perfectly resolve and precise representations of both the gradual vertical and horizontal variations of velocity with depth.

The SRT method uses the inversion algorithms to achieve a 2D velocity section for the subsurface beneath the seismic line by using the soils/rock return to the seismic energy from the source (Hiltunen and Cramer, 2008; El Hameedy *et al.*, 2023). SRT resolves shallow depth “inhomogeneities” in velocity distribution with good resolution and high accuracy with abrupt “lateral discontinuities” and gradients (Bery, 2013; Al-Saigh and Al-Heety, 2018; Baban *et al.*, 2023).

Many investigations over the past years (e.g., Gamal and Hanafy, 2004; Sheehan *et al.*, 2005; Hiltunen and Cramer, 2008; Kanli, 2009; Cardarelli *et al.*, 2014; Azwin, *et al.*, 2013; Khalil and Hanafy 2016; Al-Heety, 2018b; Abudeif, *et al.*, 2023) have noted that SRT applications are successful in conditions where typical refraction techniques did not succeed, for example velocity distribution with both vertical and lateral velocity gradients. These kinds of applications have also been used for civil engineering aims. Nevertheless, almost all such studies use a sequential strategy to gather compressional- and shear-wave refraction data, or use refraction and surface wave techniques cooperatively (Uhlemann *et al.*, 2016; Pegah and Liu, 2016). Consequently, the shear refraction method allows us to measure the velocity of the horizontal polarization component of shear-wave (VsH). The MASW technique is based on surface wave analysis methods to extract the vertically polarized component of the shear wave velocity (VsV) (Al-Saigh and Al-Heety, 2014; Shakir *et al.*, 2013).

Aim of study

The aims of this paper are as follows: (1) to analyze Vp and Vs using a P and SH tomographic processing method, (2) to investigate the site and evaluate the spreading of the subsurface soil/rocks, and to deliver information about the geotechnical parameters of the shallow soil/rocks at the proposed site University of Baba Gur-Gur in Kirkuk City.

Geographical Location and Geology of the Study Area

The survey site is situated about 11 km northeast of Kirkuk Governorate. Away about (1.0 km) from the Khas'sa Soo River and beside (about 150 m) to Kirkuk ring and Sulimani-Kirkuk roads as shown in (Fig. 1), it lies at crossed latitude ($35^{\circ}29' N$) and longitude ($44^{\circ}25' E$) with elevation around (400 m) above sea level. The area under study is characterized by a flat terrain. Tectonically, it is located within the low folded zone (LFZ) according to Jassim and Goff (2006). From a stratigraphic viewpoint, the studied region is characterized by the presence of a variety of geological formations, generally extending from the Middle Miocene to the Pleistocene periods (Sissakian and Al-Jibouri, 2012) as seen in Figure (2). The Fat'ha, Injana, Mukdadiya and Bai Hassan formations are the dominant stratigraphic formations that have been extensively exposed or are present in the subsurface within and surrounding study area. In addition, another distinct types of Quaternary clastic sediments are found in some places around the area of study (Sissakian *et al.*, 2015). The Fat'ha Formation (Middle Miocene) mainly consists of alternating beds of red claystone, brown or green marl, gypsum, anhydrite, and salt. These strata alternated as well with limestone, marl, and fine-grained clastic sediments. The Injana Formation (Late Miocene) is mainly composed of brown mudstones and siltstones that alternate with coarse- to medium-grained sandstones. The top contact exhibits a gradual transition between the Injana and Mukdadiya formations, characterized by an appearance of pebbly or gravely sandstone. The Mukdadiya Formation (Late Miocene-Pliocene) is characterized by cycles of sedimentation that have transition from coarser gravely/pebbly sandstone to finer red mudstone, grey claystone, and brown siltstones (Sissakian *et al.*, 2015). This can be seen in Figure (3). The sandstones in the interested site exhibit significant cross-bedding and are associated with channel lags. Sandy clay soils, mainly derived from the Mukdadiya Formation, characterize the study area and are characterized by the occurrence of clay balls. The Bai Hassan Formation, mainly consists of sediments from the Pliocene-Pleistocene period, are partially overlain by polygenetic sediments of Quaternary age. The field study exhibits various Quaternary sediments such as Pleistocene and Holocene deposits. For instance, Pleistocene River terraces have formed along the Khas'sa Soo River, mainly composed of sand, clay, and pebbles (Al-Gburi *et al.*, 2023). Figure (3) shows the distribution of lithological units at the borehole inside the study area.

Materials and Methods

Shallow Seismic Refraction Tomography Method

Refraction tomography is capable of accurately determining velocity gradients and lateral velocity variations. It is especially helpful in geological settings where traditional refraction

methods are unnecessary (Hiltunen and Cramer, 2008; Metwally *et al.*, 2017; El Hameedy *et al.*, 2023). The main results of this strategy are the velocities, thicknesses and depths, and soil/rock condition. The efficacy of P-wave and horizontal shear (SH) wave refraction in measuring the depth of the bedrock has been established in site characterization investigations (Bery, 2013). The integration of compressional and shear refraction methods enhances our understanding of subsurface geology and supplies additional information. Variations in elastic moduli, porosity or saturation have distinct effects on P- and S-waves make them essential for distinguishing different lithological compositions (Mohammed *et al.*, 2020; Abudeif *et al.*, 2019). In our case, we need to know the geomorphology of the bedrock, as well as to categorize the soil/rock beds using the nearby borehole dataset and outcrops which provide lithological data needed for seismic interpretation. The current study discusses SRT application consisting of several lines to characterize the soil/rock layers velocities, thickness, bedrock depth, and topography. Based on the interpretation of 2D seismic tomograms, as well as from (V_p , V_s , density), the corresponding dynamic and elastic moduli have been calculated.

P- and SH-wave SRT Data Acquisition

The geophysical survey involves compressional (P) and shear (SH) seismic wave refraction data recording followed by data processing steps and tomography inversion. The seismic acquisition setup is deployed P-recording and then SH-recording at the sites of the same profiles during May 2018. The compressional (P) and shear (SH) data are gathered at four parallel lines in the survey site, all lines-oriented NW–SE (Fig. 1).

The seismic data are recorded on twelve channels *ABEM Terraloc MK6*. The total length of every line is 75 m and it is combined of (2) overlapped arrays (forward and reverse) with center shots, 6 shots in total for each line. To measure the compression (P) and shear wave (SH) data, we have used vertical and horizontal geophones (10 Hz) respectively. The total geophones number in each array is 12 geophones with an inter distance of 5 m. The length of each array is 55 m, with an array overlapping distance of 20 m. The shot points are placed at both ends on (-2.5 offset) and in between the middle spread length between geophones 6 and 7 (at 27.5 m) and (at 57.5 m). The seismic survey lines are carried out with a 10 m line interval. The sampling interval is 500 μ s and the sampling rate is 0.50 μ s with a total record length of 1024 ms for both P- and SH-wave refraction acquisitions. Figure (4) shows the layout of the P- and SH- seismic refraction survey. A 7.5 kg sledgehammer is employed as a seismic source of energy for generating P- and S-wave. For each recording, 5 to 10 times stacked shots are made at each shot point position to increase the SNR. For the compressional refraction, the steel plate is struck vertically by a sledgehammer, whereas for shear refraction data, a wooden rod is struck horizontally.

Generally recording of the SH-wave is sensitive because the shear-wave has well-known issues such as generation and picking in SH-refraction methods (Xia *et al.*, 2002). Two separate shots for the SH-refraction survey are recorded at every single shot position from opposite sides to generate SH-polarized waves vertical to the seismic line direction to assist picking arrival times. Table (1) summarizes the data acquisition parameters.

Table 1: Data acquisition parameters.

Setting	Parameters	Setting	Parameters
Acquisition Seismograph System	Terraloc MK.6 (12 Channel)	Array Dimension (D)	55 m
Source	Sledgehammer (7.2Kg)	Profile total length	75m
Receiver (Geophones)	10 Hz V and H geophones	Source Offset (X1)	2.5 m Source
Number of Receiver (N)	12 geophones	Sample interval (dt)	0.250 (msec)
Receiver Array	Linear (overlapping)	Record length (L)	1 Sec.
Receiver Spacing (dx)	5 m	Stacks per each shot location	(5 to 10) stacks

Data Processing and Tomography Inversion

First break picking

The obtained seismic datasets (forward, middle, and reverse) are analyzed using *SeisImager/2D* software offered and developed by *Geometrics Inc.* and OYO Corporation (2019). Six group record file lists are created, each contains a seismic record acquired at every

line. The raw data are pre-processed in *Pickwin* modules for each file list including the shot positions and the offset between the geophones defined. After the geometry array is updated, the shot records are filtered using a band-pass (BP) filter to remove noise. Although the BP assistances in the picking process, it also yields artifacts at early first-arrival times. After visual validation with software, the first break times (FB) are picked from P- and SH-waves shot records semi-automatically and manually for all shot positions. The FB error is about ± 0.95 ms defined by manual iterated FB of the data. Figure (5) shows raw data and first-break picking of SRT-1.

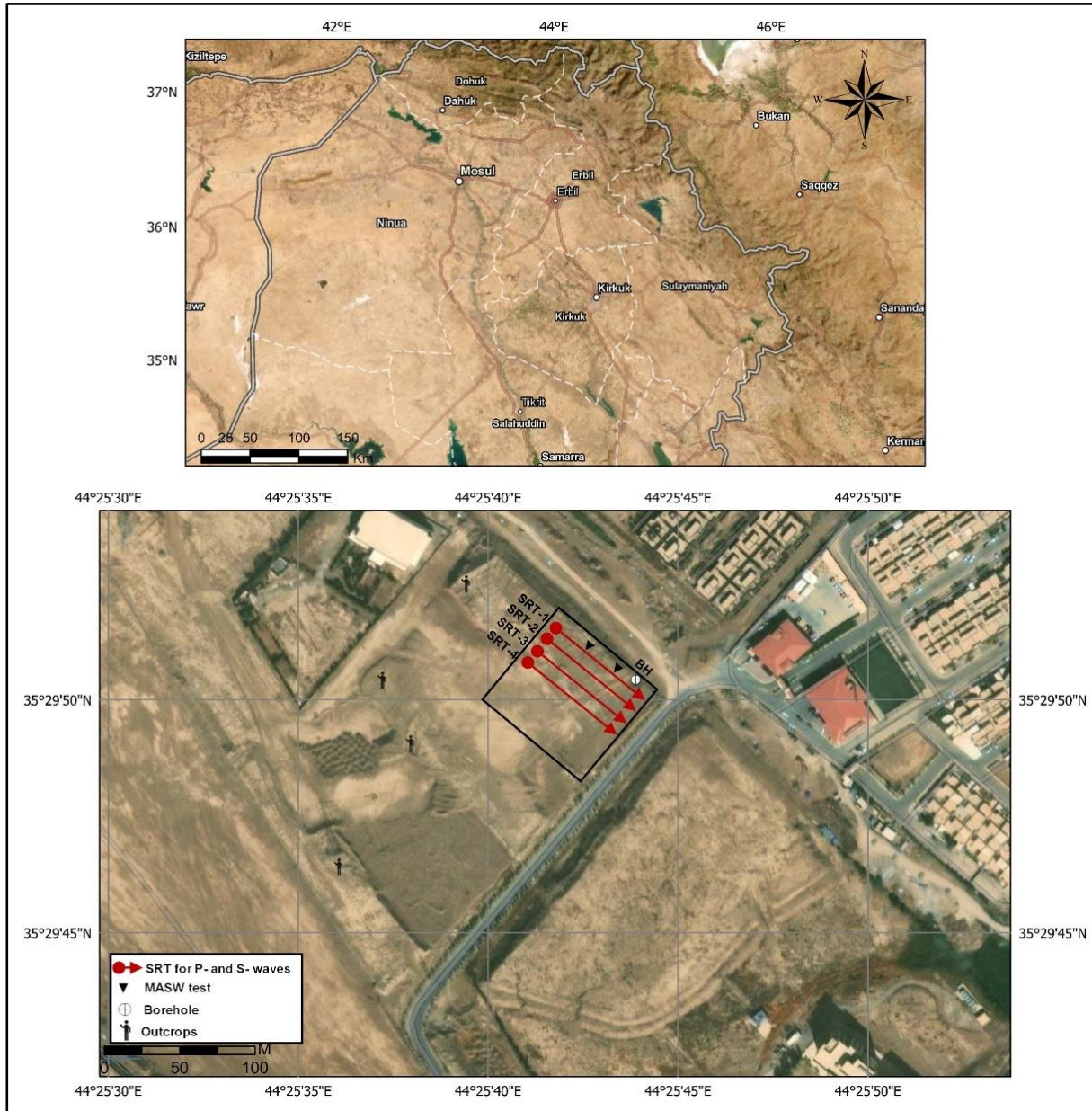


Fig. 1. The study area Location on Google Earth satellite image showing the locations of SRT (thick red arrow lines) and MASW survey profiles (black triangle), borehole location (white cross circle), and geological outcrops around the survey area.

The first-arrivals (or FB) of the compressional- and shear waves are picked for each record. Then, the picked results are plotted with the offsets between geophones to create the travel time–distance (t - x) curves for each shot location. Plotrefa module is used to produce the (t - x) curves for all the shots along each line. The (t - x) curves are exposed and scanned, and the selected from them are adjusted (manually) for more accurate data interpretation. The Travel time curves must be improved and examined to deliver a correct estimate of compressional- and shear-wave velocity structure (Sheehan *et al.*, 2005).

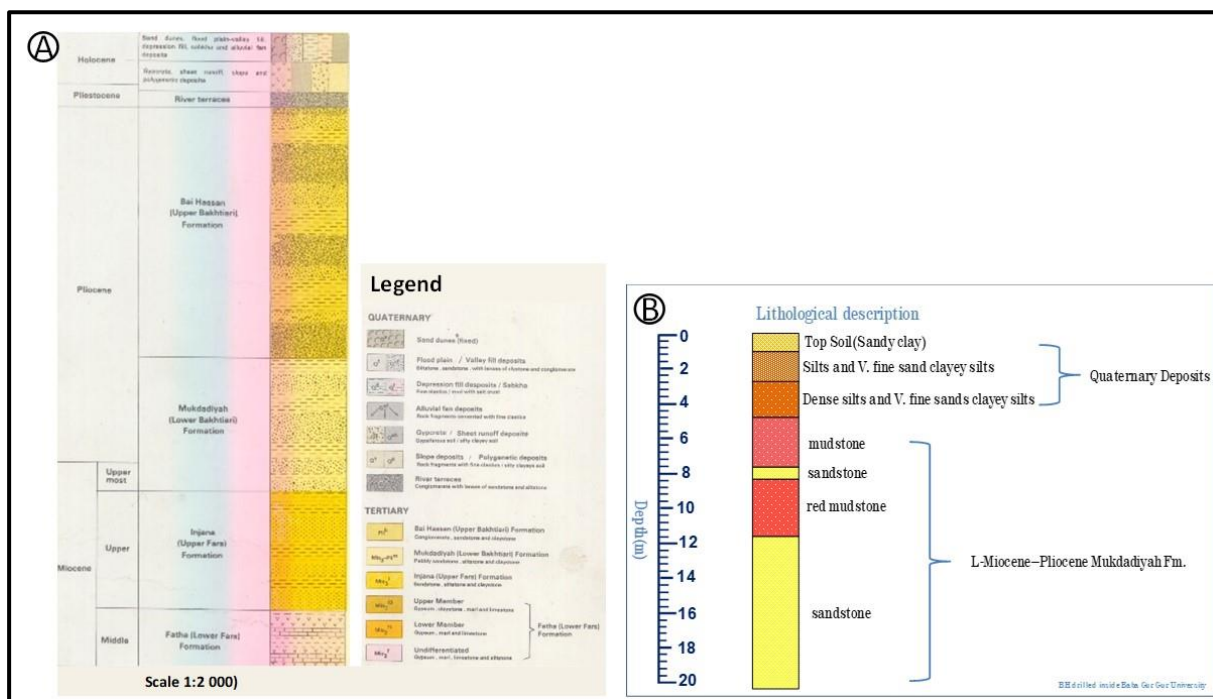


Fig. 2. A. Stratigraphic column of the study region (Sissakian *et al.*, 1993); (B) Borehole lithology description showing lithological units. These units will be correlated to geophysical survey results. The locations of boreholes are on Google Earth image (Fig.1).

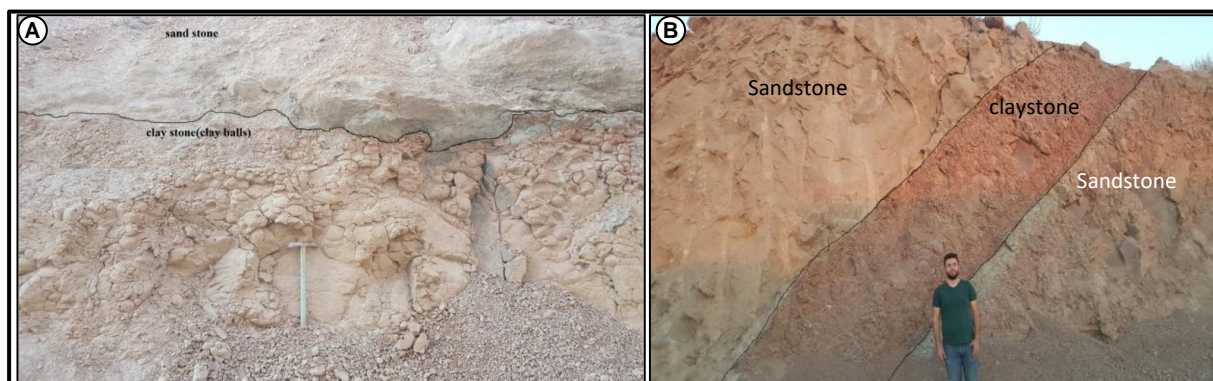


Fig. 3. Mukdadiya Formation outcrop observed in the study area, (A) with strike-slip; (B) with dip direction.

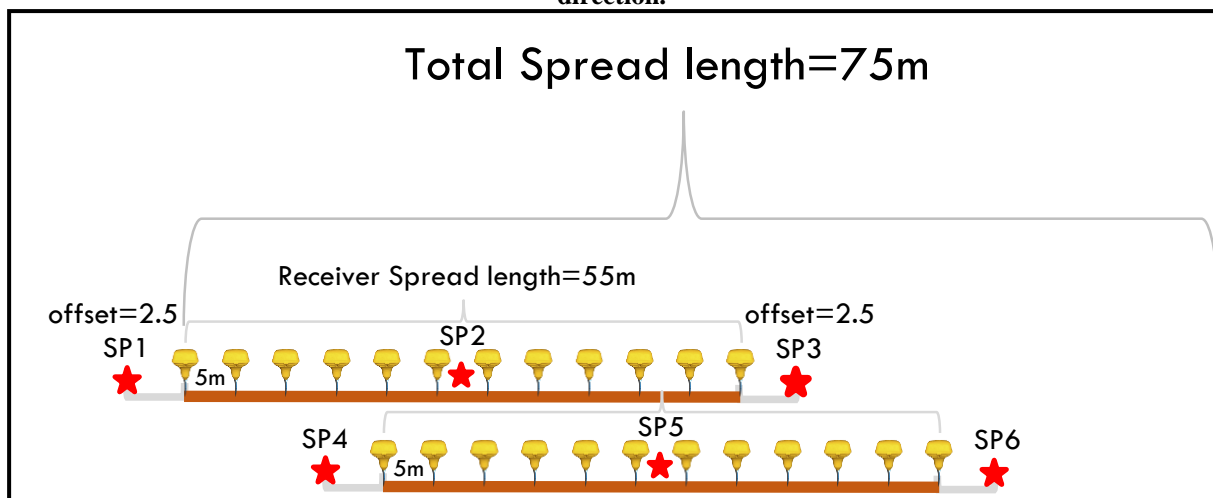


Fig. 4. Layout of the P- and SH- waves shallow seismic refraction survey.

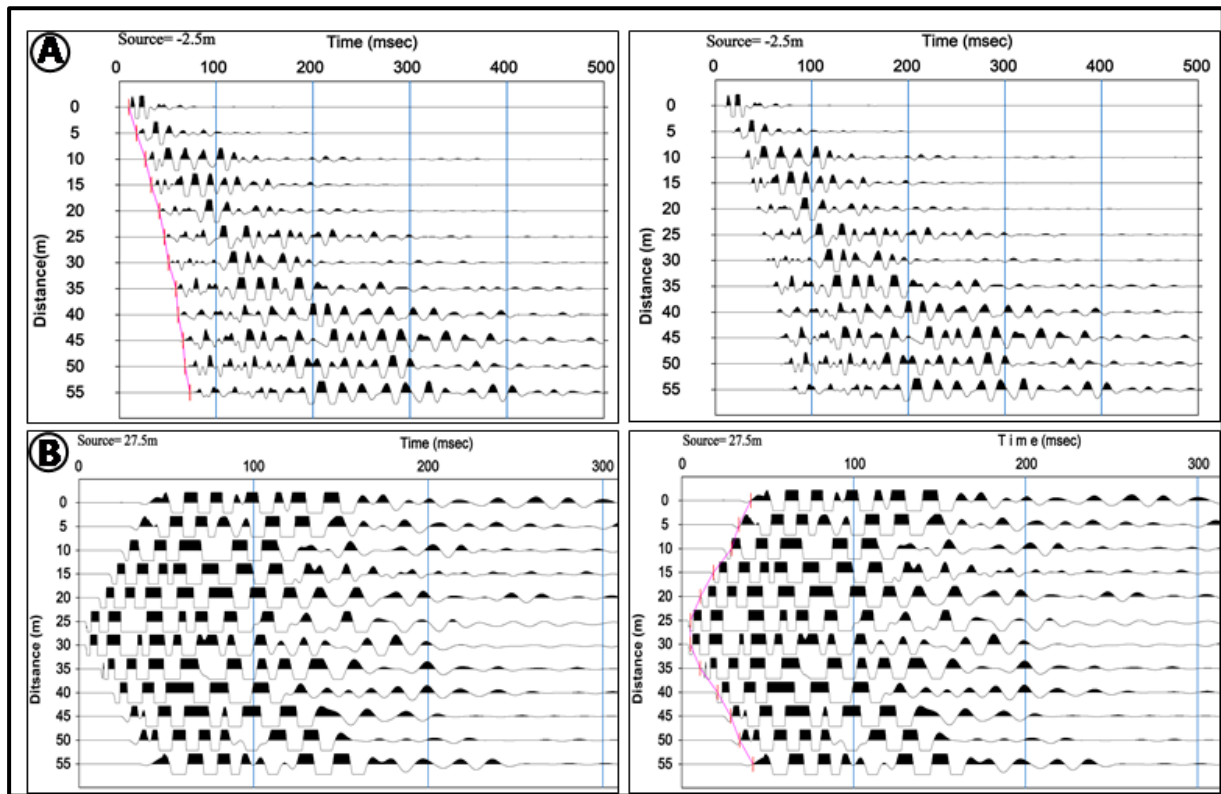


Fig. 5. Examples of the shot record of the seismic SRT-1; (a) normal shot, (b) center shot and corresponding picking first break. The seismic traces are normalized, and abnormal amplitudes are trimmed, hence the first arriving wave with a low amplitude could be detected.

SH-waves Data quality

A sledgehammer strikes a wood rod from the opposite side as a seismic source for S-waves. Conversely, it needs further processing phase. This is reached by subtracting or adding the shots of the two opposite sides. As the wood rod is angled vertically to the receiver array, just the shear wave (S_H) resolved and evaluated in the subsequent, supposing an “isotropic” shear wave propagation (Uhlemann *et al.*, 2016).

It is crucial to be aware that inconsistencies between shots taken from different directions might lead to a degraded signal. The quality of the raw data for SH-waves is mostly good to very good, although the relatively substantial attenuation is resulted from the very soft medium. The seismic quality could be enhanced by two key steps: first, stacking multiple shots from each side of the wood rod; and second, including an additional stack. The main stack of shots from the separate wooden rod sides is determined through an examination of the correlation coefficient ρ_{xy} between each of the seismic traces x and y . The correlation coefficient ρ_{xy} is defined by Uhlemann *et al.* (2016) as

$$\rho_{xy} = \frac{\sum_{i=1}^N (x_i - \bar{x})(y_{i+\tau} - \bar{y})}{\sigma_x \sigma_y}$$

Where, (N) is the number of samples, (σ) is the variance, and (τ) is a lag.

If two opposite record traces show $\rho_{xy}=1$, the seismic traces are matching. “Correlation coefficients” are computed for every couple of the two shots, and a stacking threshold of $\rho_{xy} > 0.87$ was utilized. Traces were preserved only if at least two of the three correlation coefficients were $\rho_{xy} > 0.87$. If data are obtained from both sides after this step, SH components are picked. Over 91% of the data met this criterion. The utilization of these procedures greatly enhanced the accurate detection of the SH-refracted waves, which are the first arrival for S-waves as seen in Figure (6).

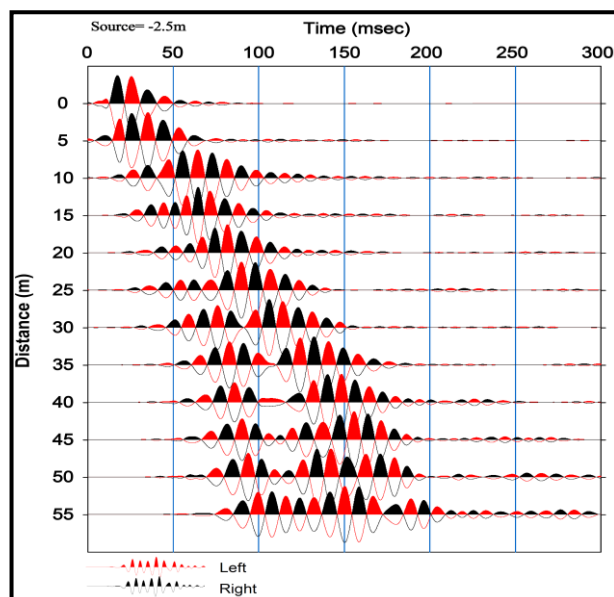


Fig. 6. Recording process of polarized SH-waves; two opposite sides recorded reversed polarity (reversed energy source) S-wave displayed in Shaded black (one polarity) and Shaded red (opposite polarity) trace mode.

Tomography Inversion

The tomography inversion for each dataset (P- and SH) is utilized by the *Plotrefa* program, which uses non-linear traveltimes tomography (Zhang and Toksöz, 1998; Geometrics, 2009). Comprising the use of raytracing for forward modeling (FD) and a “simultaneous iterative reconstruction” (SIRT) method for tomographic inversion. The method used for generating the subsurface velocity sections is fully discussed in Hayashi and Takahashi (2001).

The Tomographic inversion algorithm requests a start velocity model to begin with. The start model can be constructed in 2 techniques (Sheehan et al. 2005; Geometrics, 2009) firstly by transforming the outcomes from the time-term procedure involved in *Plotrefa*, or by creating a 2D initial model by a user-defined key of the predictable velocity, number of layers, and depth to the deepest layer. In either case, the software will create the velocity distribution and geometry for the start model.

For the current study, the start model is generated on the basis of analysis of (t-x) curves and available borehole data. However, the minimum and maximum Vp or Vs velocities are calculated using the *Plotrefa* velocity function. The inversion technique begins with the generated start model and iteratively ray trace within the model with the main goal of decreasing the “root mean square error” (RMSE) between the calculated and observed (measured) travel times to construct a velocity model with small-scale artifacts. The velocity model is restructured and the latest calculated (t-x) curves are constructed and matched to the data. This process is iterated till the lowest possible RMSE is reached within a chosen number of iterations. The result of the submission of the tomographic method is a two-dimensional Vp and Vs of the near-surface beds in the path of the line. The RMSE between the observed and calculated values for all the tomographic sections is (≤ 5.0 ms) which provides high reliability of the results.

Results and Discussion

Compressional and Shear Wave Tomography

The Vp and Vs final inverted SRT velocity sections using linear geophones array with overlapping configuration acquired in this study show a good fitting with an RMSE of 2.68 to 5% ($\text{RMSE} \leq 5\%$) between measured and calculated velocity after (7 to 10) iterations. The inverted velocity sections show mostly very low velocities to relatively high velocities. The Vp and Vs values variations from 290 to ≥ 2500 m/sec, and 110 to ≥ 1150 m/sec, respectively. A particular analysis of both Vp and Vs models shows that the greatest obtained depth is about 20 meters; moreover, we can clearly distinguish four geo-seismic layers in all cross-sections. The interpreted Vp and Vs velocities and depth sections for SRT-1, SRT-2, and SRT-4 velocity

sections are presented in Figures (7 and 8). The lowest velocities in the Vp tomograms (about 300 m/s) are found (~ 1 m) below the ground surface in all acquired profiles. On another hand, the Vs tomograms show that the lowermost velocities (Vs= 150 m/s) are detected at the same depth (~1 m). A sharp increase in seismic velocities can be found just below and to the end depth of SRT sections.

The strong boundary shown in the Vp tomograms is less obvious in the Vs sections exhibiting a slightly greater depth and demonstrating smaller variations in velocity. Furthermore, all profiles show a significant irregularity in S-wave velocity at greater depths, although it is not as noticeable as the anomaly seen in the Vp sections. The detected characteristics in both the Vp and Vs velocity tomograms show remarkable spatial consistency.

The Vp boundary of each layer is identified based on the correlation with available lithological data (borehole and outcrops) near the survey site (see Fig. 2). The upper low Vp layer is correlated with the silty clay soils recorded in the borehole (BH-1) and recognized in the field, whereas the deep-seated high Vp layer is attributed to the sandstone response considering the closest geological outcrop which belongs to the Mukdadiya Formation. According to the outcrop, field density, and Vp, the first layer is described as soil (competent and sometimes loose soil), the second layer is described as a sand layer from Mukdadiya Formation, while the third layer is described as a silt layer from Mukdadiya formation, and the 4th layer is described as a clay bed from Mukdadiya Formation too as shown in Figure (8A). SH-refraction tomography (Fig. 8B) is shown in conformity with the Vp tomography. The topsoil layer has a low velocity between 110 and 115 m/s. The Vs values are in ranges of (310 to 325 m/s) and depths ranging from (3.0 to 4.0 m) depicting the second layer. The 3rd layer, with Vp value ranging between (685-675 m/s), covers a depth between (6 and 11.5 m) and covers a stiffer layer with Vs values >1150 m/s. These results are in agreement with the adjacent drilled boreholes inside the survey area. The results of the surveyed seismic lines such as thickness, depth, Vp, and Vs values for the four layers are given briefly in Table (2).

Table 2: Vp, Vs, and thickness and depth values for four layers results from SRT.

	1 st layer	2 nd layer	3 rd Layer	4 th layer
Vp (m/sec)	290-320	830-870	1530-1600	2450-2535
Vs (m/sec)	110-125	310-330	675-690	1150-1160
Thickness(m)	0-1	3-4	3-7	N/A
Depth to the top (m)	≤ 1	3-5	6-11	N/A
Interpreted Lithology unit	sandy clay	Silts, dense silts, very fine sands clayey silts	Mudstone	Sandstone
Formation	Top soil	Quaternary deposits	Mukdadiya	Mukdadiya

MASW-Based Refraction Method Test

Numerous engineering and geophysical approaches are applied to determine the in-situ Vs values; e.g., the SH-refraction method measures Vs fluctuations beneath 2D profiles. Further methods of assessing shear-wave changes with depth at only one point surface location offer a one-dimensional (1D) velocity-depth profile. The 1D profile shear wave velocity-depth is computed by dispersion curves (DC) iterative inversion, which is obtained by frequency-velocity transformation technique from the recorded data (Xia *et al.*, 1999; Park *et al.*, 1999 and 2000). The approximation of shear wave velocity is commonly accomplished in a relatively indirect simple manner using surface-wave approaches as an alternative to SH-refraction (e.g., Park *et al.*, 1999).

Obtaining Vp and Vs values from one measurement setup is attractive due to the possibility of preserving time and reducing tool costs, still though SH-wave strategies deliver results of high quality. In addition, Pasquet *et al.* (2014) conducted an assessment of the feasibility of using both SH-refraction tomography and MASW inversion each other to characterize Vs.

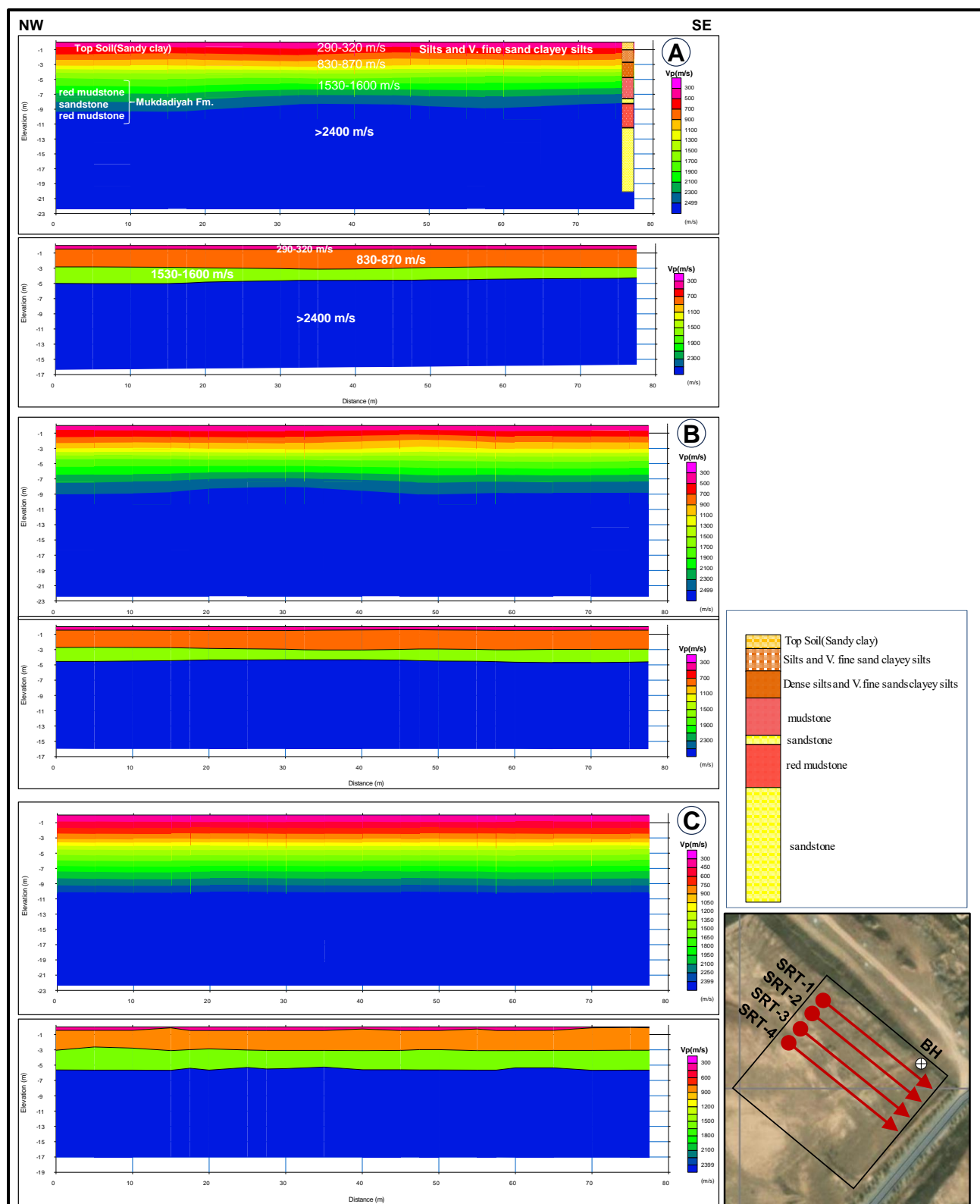


Fig.7. P-wave tomography inversion and depth model for (A) SRT-1 (rms 2.68 after 7 iterations); (B) SRT-2 (rms 3.72 after 9 iterations); and (C) SRT-4 (rms 4.94 after 10 iterations).

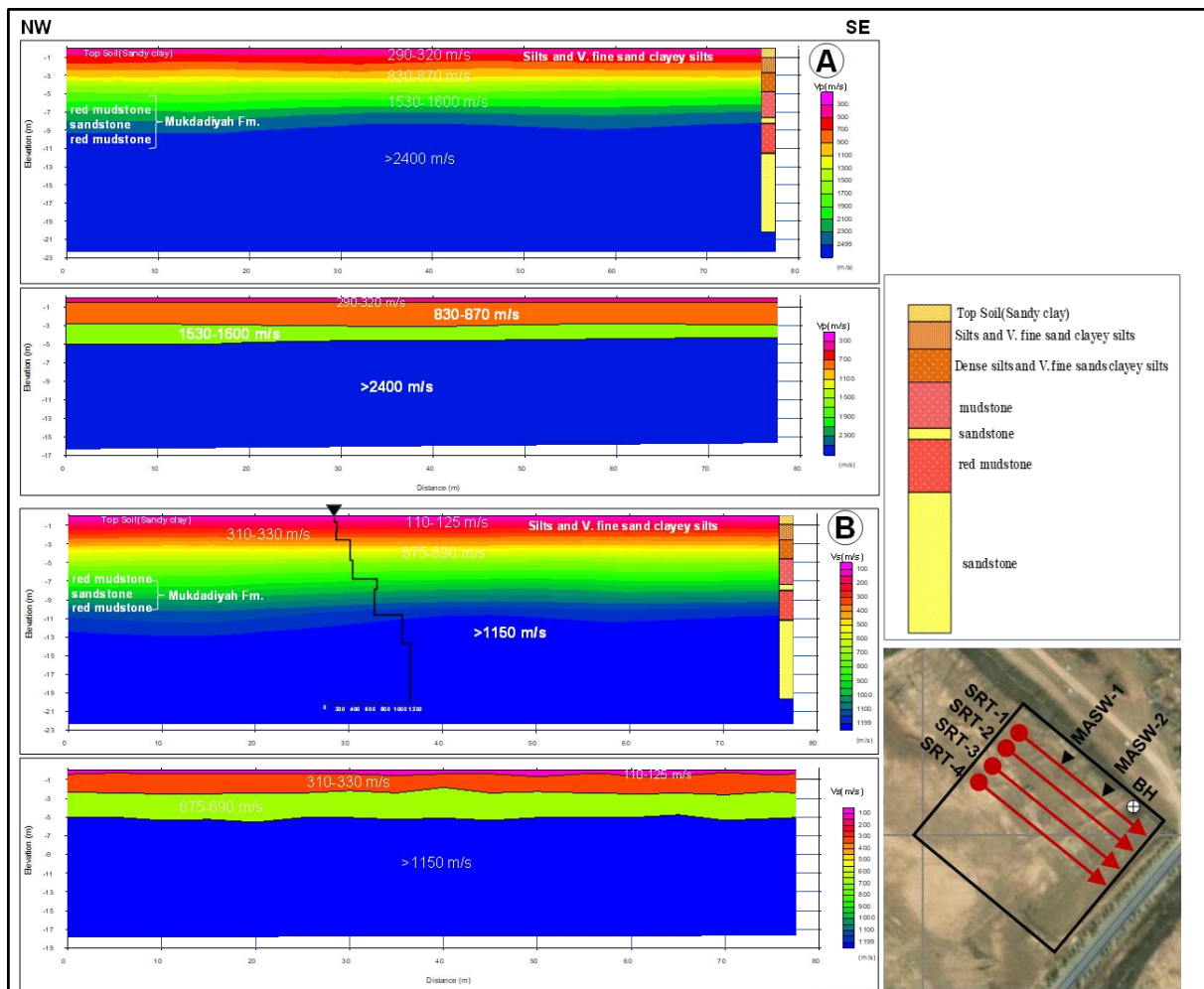


Fig.8. P- and SH-wave tomography inversions and depth model for (A) P-wave SRT-1(rms 2.68 after 7 iterations); (B) SH-wave SRT-1 (rms 4.79 after 8 iterations. For location, see inset map.

MASW experiments test are achieved in the current study to determine the 1D Vs profile using the MASW-based P-refraction method. In the MASW test, a standard P-wave recording equipment is used to produce an average 1D Vs profile. Also, we use the results of SH-refraction and MASW tests to assess whether this method can be alternated with SH-refraction for shallow soil and rock characterization. MASW tests are conducted along two seismic arrays with 12 vertical geophones (10 Hz), which can offer surface-wave phase velocities at frequencies as low as (e.g., ≤ 10 Hz), and high as (40 Hz). The array length is 55 m with a 5m offset before the first geophone to avoid near and far-field effects, with vertical stacking (5-10) shots to considerably reduce ambient noise. The 1D MASW processing and inversion work flow is shown in Figure (9).

To calculate the 1D Vs model, SeisImager/SW software (Pickwin and WaveEq) is employed. The data processing forwarded through the transformation shot gathers records from the time ($t-x$) domain to the frequency-phase velocity ($f-v$) domain. The frequency range of 5-45 Hz has been chosen for the dispersion image. Figure (10) shows the produced dispersion image after the transformation. This step is followed by picking (or estimating) dispersion curves (DC) of the fundamental-mode surface waves, generally more powerful in comparison to other (higher) modes. The created DCs for each location are imported into the *WaveEq* module for further modification, quality control (QC/QA), and processing. Following that, a theoretical start model is produced through the depth conversion result from the program, which is accomplished as an initial benchmark for the inversion procedure. Finally, the inversion process is executed via a least-squares inversion algorithm (Xia *et al.*, 1999). The outcome of this practice is a 1D shear wave-depth profile that corresponds to the midpoint of each seismic

line. In other words, every 1D shear wave profile expresses the median property within the receiver array below a one-point location measured to be at the spread center (Xia *et al.*, 2000).

Two tests of the 1D Vs-depth profile produced from the MASW record are measured near the drilled boreholes at the SRT-1 seismic lines as shown in Figure (11). The MASW model as seen in this figure shows mostly lower velocities (100 and 280 m/s) than the tomographic model; and in contrast, the 1D Vs shows inverted velocity zones. The 1D Vs profiles are visually inspected and compared to the Vs values produced from refraction data at tested locations and borehole logs. The test results display good agreement. Hence, the results validates that the MASW survey could be an alternative to the SH-refraction when the near-surface conditions and survey target allow. Moreover, MASW tests have shown that standard SRT tools can produce precise surface-wave dispersion information and finally Vs profile from MASW.

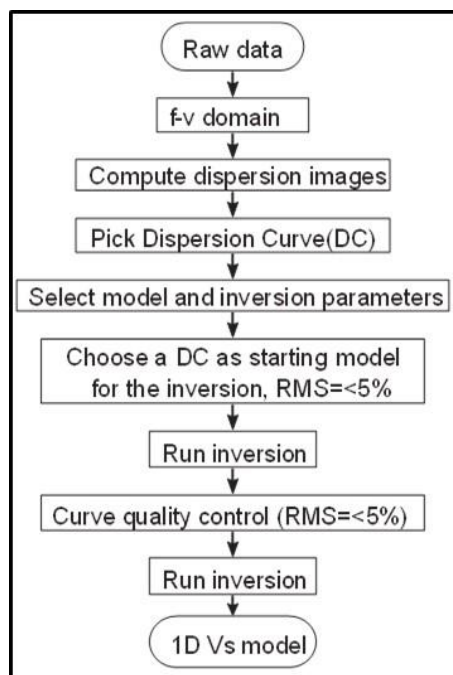


Fig. 9. 1D MASW processing and inversion workflow.

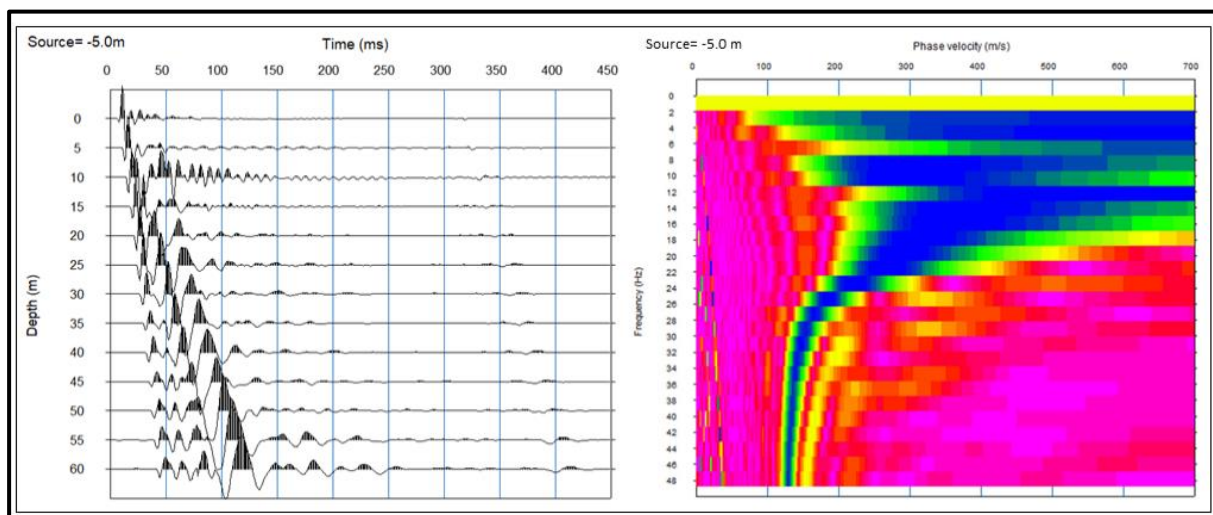


Fig. 10. Shot record (time domain) and corresponding dispersion image after transformation (frequency domain).

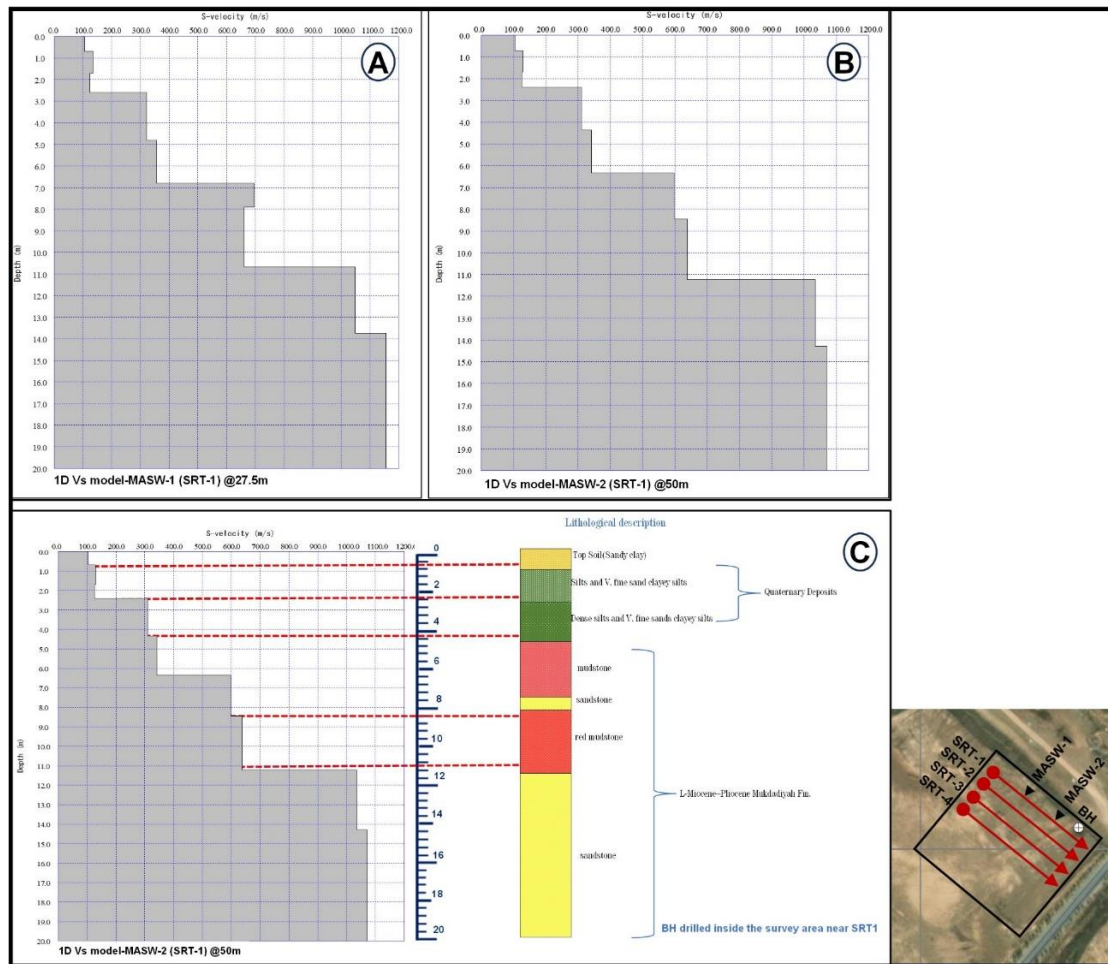


Fig. 11. Two 1D shear wave velocities Vs depth profiles obtained from MASW (A and B). (C) 1D Vs profile (MASW-2) above SRT-1 correlated with borehole log. The rms value for MASW-1 and MASW-2 are (4.85 and 3.94) respectively.

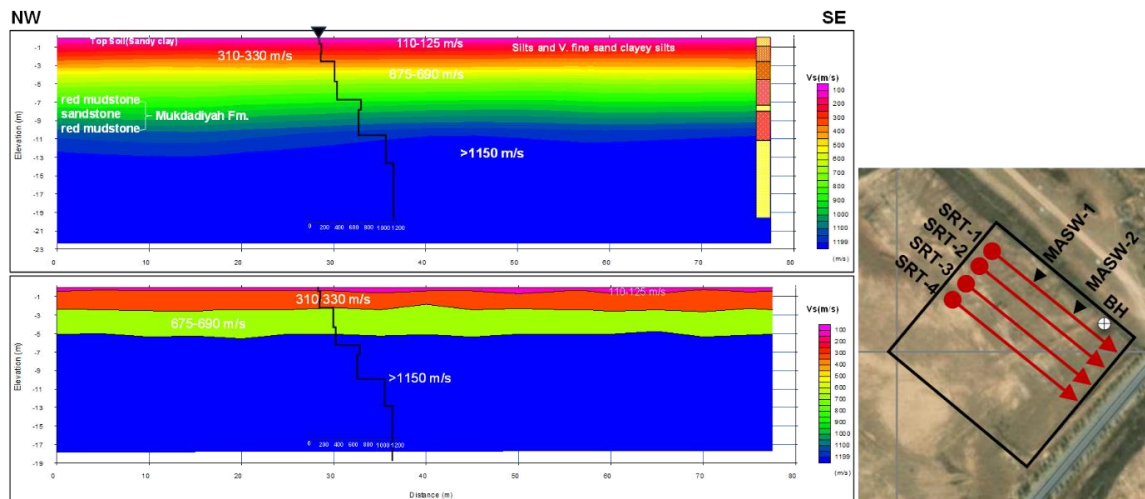


Fig. 12. 1D Vs profiles from MASW-2 overlaying SH-SRT-1. The profile shows good matches with SH-refraction shear-velocity results and borehole log. (For location see inset map). The black triangle shows the location of the MASW test.

Calculation of the Elastic and Geotechnical parameters

The combination of V_p with V_s can allow a more complete site characterization compared with using single data sets. V_s , V_p , and density can estimate some of the geotechnical parameters (Al-Heety *et al.*, 2016). The stiffness of lithology is expressed as a measure of the ability to resist deformation (Sheriff, 2002), and is ultimately linked to the material's dynamic elastic moduli that express the material's behavior under stress. Between the three main types of moduli: Young's (E), shear (μ), and bulk (β), the first two (E and μ) are commonly used

because of what they describe. Young's modulus states the deformation tendency along the axis of stress, while the shear modulus indicates the tendency of shape deformation, i.e., shearing (Park *et al.*, 2018). Corresponding to the theory of elasticity (Sheriff and Geldart, 1995), these two moduli can be expressed by a material's density (ρ) and both seismic velocities (V_p and V_s) or by Poisson's ratio (δ) as shown in Table (4). Hence, by estimating these three parameters (ρ , δ , and V_s) separately, the stiffness of various subsurface strata may be computed with high accuracy.

Poisson's ratio depends on V_p/V_s , which is related to lithology, heterogeneity, degree of consolidation, clay content, porosity, and water saturation as the rock matrix's shear modulus controls V_s . In contrast, V_p is controlled by both matrix and pore/fracture filling material (bulk and shear moduli) for a given density (Bhowmick, 2017). In the current study, V_p , V_s and field density (ρ) values are used to estimate a number of geotechnical parameters (e.g., elastic and geotechnical characteristics) to assess subsurface materials of the investigated site. Table (4) provides an overview of the empirical equations of elastic and geotechnical parameters used in the current study. Table (5) shows the results of all these parameters calculated depending on the V_p , V_s and density values.

Table 4: Elastic and geotechnical parameters empirical equations.

Parameter	Used equations	Reference
Porosity (Φ)	$\Phi = -0.175 \ln(V_p) + 1.56$	(Watkins <i>et al.</i> , 1972)
Void ratio (e)	$e = \Phi/(1 - \Phi)$	El Sharawy <i>et al.</i> , 2016)
Rock density (ρ)	$\rho = aV_p^{0.25}$ or $\rho = 0.44V_s^{0.25}$ a = 0.31	(Gardner <i>et al.</i> , 1974; Keceli, 2012)
Poisson's ratio (δ)	$\delta = \frac{1}{2} \left[1 - \frac{1}{(V_p/V_s)^2 - 1} \right]$	(Salem, 2000)
Young's modulus (E)	$E = \rho \left[\frac{3V_p^2 - 4V_s^2}{\left(\frac{V_p}{V_s}\right)^2 - 1} \right] = 2\rho V_s^2 (1 + \sigma)$	Kearey <i>et al.</i> , 2002)
Bulk modulus (β)	$\beta = \frac{E}{3(1-2\sigma)}$	(Toksöz, <i>et al.</i> , 1976)
Shear modulus (μ)	$\mu = \left[\frac{E}{2(1+\sigma)} \right] = \rho V_s^2$	(Toksöz, <i>et al.</i> , 1976 ; Kearey <i>et al.</i> , 2002)
Concentration index (Ci)	$Ci = \left[3 - 4 \left(\frac{V_s^2}{V_p^2} \right) \right] / \left[1 - 2 \left(\frac{V_s^2}{V_p^2} \right) \right]$	(Abd El-Rahman 1991)
Material index (V)	$V = \frac{3 - (V_p/V_s)^2}{(V_p/V_s)^2 - 1} = (1 - 4\delta)$	(Abdel-Rahman <i>et al.</i> 1994; 1989)
Stress ratio (Si)	$Si = 1 - 2(V_s/V_p)^2$	(Abd El-Rahman 1991)
The Ultimate Bearing Capacity (Q_{ult})	$\log Q_{ult} = 2.932(\log V_s - 1.45)$	(Abd El-Rahman 1992)
SPT (N-value)	$V_s = 89.9 N^{0.341}$	(Imai, <i>et al.</i> , 1976; Stümpel, <i>et al.</i> , 1984)
V_s^{30}	$V_s^{30m} = 30 / \sum (di/V_{si})$ (di) total thickness, and (V_{si}) of layer	IBC 2000, Eurocode 8:(2005).

Table 5: Summary of the estimated elastic and geotechnical characteristics of the soils and rocks.

layer	Vp m/s	Vs m/s	ρ g/cc	ρ ^(exp) g/cc	Φ	e	δ	E Mpa	μ Mpa	β Mpa	Ci	Mi	Si	N	Qu	
Minimum	1	290	110	1.42	1.40	0.57	1.31	0.416	48.83	17.24	96.85	3.40	-0.66	0.71	2	5.0
	2	830	310	1.85	1.81	0.38	0.62	0.419	493.63	173.9	1015	3.38	-0.67	0.72	37	110
	3	1530	675	2.24	2.15	0.28	0.38	0.379	2702	979.6	3726.8	3.63	-0.51	0.61	>50	1086
	4	2450	1150	2.56	2.30	0.19	0.24	0.359	8265.7	3041.7	9750.0	3.78	-0.43	0.56	>50	5184
Maximum	1	320	125	1.47	1.43	0.55	1.22	0.410	63.1	22.34	116.6	3.43	-0.64	0.70	3	7.8
	2	870	330	1.88	1.84	0.38	0.6	0.416	567.45	200.38	1125.5	3.40	-0.66	0.71	45	133
	3	1600	690	2.26	2.15	0.27	0.37	0.385	2836.9	1023.6	4139.1	3.60	-0.54	0.63	>50	1159
	4	2535	1160	2.57	2.40	0.18	0.23	0.367	8833	3229.4	11117	3.72	-0.47	0.58	>50	5318
Average	1	305	117	1.44	1.42	0.56	1.27	0.412	55.92	19.8	106.7	3.42	-0.65	0.70	2.4	6.58
	2	850	320	1.86	1.85	0.38	0.61	0.417	530.54	187.15	1070	3.40	-0.67	0.71	41	121
	3	1565	682	2.24	2.1	0.27	0.38	0.382	2769.5	1001.6	3933.	3.61	-0.53	0.62	>50	1122
	4	2492	1155	2.56	2.35	0.19	0.24	0.363	8549.3	3135.6	10433	3.75	-0.45	0.57	>50	5251

Elastic Moduli

Below is a brief of the petrophysical and elastic-moduli marks:

1. The porosity values (Φ) are between (0.56 to 0.57), (0.384 to 0.381), (0.277 to 0.285), and (0.18 to 0.193) for the four layers respectively. The 1st layer has relatively high porosity values, which may correspond to the presence of incompetent materials commonly observed in topsoil. The 2nd layer is characterized by an intermediate porosity that indicates the silts, dense silts, and very fine sands clayey silts layers (Quaternary deposits). The mudstone and sandstone deposits are revealed by the porosity that is comprised of moderate porosity materials. The void ratios (e) are between (1.22 to 1.31), (0.60 to 0.62), (0.37 to 0.38), and (0.23 to 0.24) for the four layers. The last layer is characterized by a decreased void ratio that reveals relatively more competent materials.
2. The field densities (ρ) range from (1.40 to 1.43), (1.81 to 1.84), (2.15 to 2.15), and (2.3 to 2.4) g/cc respectively, with averages of (1.142, 1.82, 2.15, and 2.35) respectively. However, the average density according to Gardner et al, (1974) and Keceli (2012) equation based on V_p or V_s is (1.44, 1.86, 2.24, and 2.56) respectively. The density data reveal an increasing trend from the first to the fourth layer implying that the fourth layer has higher density values. This may be attributed to the presence of highly competent materials and a deeper depth of burial.
3. Poisson's ratio (δ) is considered an important factor in engineering projects. The values range from (0.410 to 0.416), (0.416 to 0.419), (0.379 to 0.385), and (0.359 to 0.367) for the first, second, third, and fourth layers respectively, with averages of (0.41, 0.42, 0.38, and 0.36) respectively. The quiet competent soil/rocks occupy a greater Poisson's ratio and vice versa. The Poisson's ratio results proves that the 1st layer consists of "less competent" materials, whereas the third and fourth layers involve "fairly to moderately competent" materials. According to Table (6), the first layer, the second, and the third layer are classified as "incompetent to slightly competent", while the fourth layer is "fairly to moderately competent".
4. The Young's moduli (E) range from (48.83 to 63.1), (493.63 to 567.45), (2702.1 to 2836.98), and (8265.7 to 8833) MPa respectively, with averages of (55.9, 530.5, 2769.5, and 8549.3) respectively. The 3rd and 4th layers are notable by relatively high values.
5. The shear (rigidity) moduli (μ) range from (17.2 to 22.3), (173.9 to 200), (979 to 1023), and (2658 to 2677) respectively, with averages of (19.8, 187, 1001, and 3135 Mpa) respectively. It is concluded that the 3rd and 4th layers are "compacted" mudstone and sandstone based on the significantly high rigidity values.
6. The bulk moduli (β) range from (96.8 to 116), (1015 to 1125), (3726 to 4139), and (9750 to 11117 Mpa) respectively, with averages of (106.7, 1070, 3933, and 10433) respectively. The 3rd and 4th layers are characterized by relatively high values.

Geotechnical Parameters

Below is a brief of the geotechnical parameters results:

1. **Concentration index** (C_i): In engineering, compaction or concentration of materials for foundation purposes can be measured using (C_i) parameter. Materials with higher values are more competent, whereas those with lower values are less competent. The (C_i) values in this study range from (3.40 to 3.44), (3.387 to 3.404), (3.592 to 3.637), and (3.721 to 3.788) respectively, with averages of (3.42, 3.34, 3.60, and 3.75) respectively. Abd El-Rahman (1991) verified that (C_i) values are higher in the more competent materials (e.g., the fourth layer) and lesser in the soft ones (top layer).
2. **Material index** (M_i): This parameter is related to the content of the whole material, the quantity of consolidation, which have an influence on the wave velocities as a result of the medium of the materials (Abd El- Rahman, 1989). Sheriff and Geldart (1995) divided the derived material index values into four major categories for foundational considerations. (M_i) values for the first, second, third, and fourth layers are (-0.640 to -0.664), (-0.64 to -0.676), (-0.517 to -0.543), and (-0.435 to -470) respectively, with averages of (-0.652, -

0.670, -0.530, and -0.452) respectively. Increasing the value of this coefficient with depth indicates increasing soil hardness, whereas according to Table (7), the three top layers are classified as incompetent to slightly competent, while the last layer is classified as fairly to moderately competent.

3. **Stress index** (S_i): the behavior of this ratio noted by Bowles (1982) is like Poisson's ratio, where its value rises for the less hard (incompetent) and cohesive materials with high fluid content. The values range from (0.70 to 0.71), (0.71 to 0.72), (0.61 to 0.63), and (0.56 to 0.58) respectively, with averages of (0.70, 0.71, 0.62, and 0.56) respectively. According to the classification scale of Abd El-Rahman (1989), the three top layers indicate their less competent materials.
4. **Ultimate Bearing Capacity** (Q_{ult}) range between (5.0 to 7.85), (110 to 133), (1086 to 1160), and (5184 to 5318 kN/m²) respectively, with averages of (6.58, 121.8, 1122 and 5251 kN/m²) respectively. The results show that the first and second layers are weak and incompetent, the third layer is weak but better than the first and second layers, while the fourth layer is moderately competent and much harder than the other layers. The 4th layer has the highest values reflecting "competent" materials, while the uppermost layer has the lowest values of "competent soils". The point load test (PLT) for sandstone and mudstone samples belonging to the Mukdadiya Formation from the survey area show according to Bieniawski (1975) that the mudstone and sandstone rocks are of weak to medium strength depending on estimated values of the Uniaxial Compressive Strength (UCS) of the tested samples (≤ 50 Mpa), These results are consistent with the ultimate bearing capacity (Q_{ult}) results obtained from the shear wave velocities.
5. **Standard Penetration Test** (N-value) is computed using Imai's (1975) equation that was modified by Stumpel et al. (1984) depending on V_s values. The values of N-values for the 1st and 2nd layers are (2 to 3), and (37.7 to 41.5) respectively, with averages of (2.41 and 41.5) respectively, whereas the N-values are >50 for the third and fourth layers. According to Sheriff and Geldart (1995), the greater the SPT value, the harder it is for the rock to be penetrated; and thus, the greater the degree of "competence". In contrast to the first and second layers, which are characterized by "very soft soil" and "compacted" silts respectively. The top layer had small N-values due to weathered materials and the lessening compaction of these units. Generally, for the third and fourth layers in our area, these values increase by >50 which refer to compact clay and sandstone.

Table 6: Soil and rock quality according to Poisson's ratio and the material index (Sheriff and Geldart, 1995).

Soil description parameter	Incompetent to slightly competent	Fairly to moderately competent	Competent	Very highly competent
Poisson's ratio (δ)	0.41-0.49	0.35-0.27	0.25-0.16	0.12-0.03
Material index (M_i)	(-0.5) -(-1)	(-0.5) -(0)	(0) -(0.5)	>0.5

Table 7: Soil and rock quality according to Concentration index and the Stress ratio (Abd El-Rahman, 1989)

Soil description parameter	Weak		Fair		Good
	Incompetent		Fairly competent		Competent
	Very soft	Soft	Fairly competent	Moderate competent	Compacted
Concentration index (C_i)	3.5-4.0	4.0-4.5	4.5-5.0	5.0-5.5	5.5-6.0
Stress index (S_i)	0.7-0.61	0.61-0.52	0.52-0.43	0.43-0.34	0.34-0.25

Determination of V_{s30} for seismic soil classification

The determination of V_{s30} for near-surface geologic units is conducted following NEHRP's criteria and others (NEHRP, 2003; Eurocode-8, 2005). Soil classification results show that the investigated region is within the range of ($360 \text{ m/s} \leq V_{s30} < 760 \text{ m/s}$) and thus falls in the C category according to the UBC and EC8.

Table 8: Site categorization based on the NEHRP (2003) criteria.

Site class	Description	Average Vs (m/s) top 30 m
A	Hard rock	$V_{s30} \text{ (avg)} > 1500$
B	Rock	$760 < V_{s30} \text{ (avg)} \leq 1500$
C	Very dense soil	$360 < V_{s30} \text{ (avg)} \leq 760$
D	Stiff soil	$180 < V_{s30} \text{ (avg)} \leq 360$
E	Soft soil	$V_{s30} \text{ (avg)} < 180$
F	Soils requiring site-specific evaluation	-

Table 9: Average calculated Vs30 and site classes along with SH- refraction profiles.

Line ID	Average Vs30 (m/s)	Site Class
Line-1	490, (440 Vs MASW)	C
Line-2	512	C
Line-3	470	C
Line-4	550	C
Average	505.5	C

At last, the combination of elastic moduli and geotechnical results indicate that the fourth layer consists of competent clays and sandstone. Prior to beginning construction operations, it is crucial to consider the geotechnical metrics to be able to evaluate the level of competency for the revealed layers.

Conclusions

P-wave, SH-wave refraction and 1D MASW measurements are used to investigate the near-surface soil and rock features in the University of Baba Gur-Gur, northeastern Kirkuk. The main aims of this paper are to compute the in-situ the elastic moduli, the geotechnical properties and some petrophysical characteristics of the soils/rock's materials. Four splits seismic refraction profiles (P- and SH) and two 1D MASW locations are employed at the survey site. Four geo-seismic beds are supposed according to the horizontal and vertical change in both Vp and Vs sections. The lithology of these near-surface layers is (1) topsoil layer, which is made up of a mixture of sand and clay that are notable by a relatively high porosity ratio with a larger portion of voids and incompetent materials (2) Quaternary deposits (silts, dense silts, very fine sands clayey silts) of slightly competent to fairly competent materials (greater competent than the top layer) with intermediate porosity (3) mudstone unit and (4) sandstone unit of fairly competent materials, lower porosity and void ratio materials. The Vp and Vs values used to calculate the geotechnical parameters, also average Vs30 of the survey site are calculated for site soil and rock classification.

The cost-effective seismic refraction tomography (SRT) method shows a high degree of accuracy and clarity for the near-surface layers for geotechnical characterization over survey area. The velocity models, thickness, depth and bedrock topography underlying layers can be obtained in more details as well as for elastic moduli and geotechnical parameters evaluation. The investigated site is categorized as a (C) class according to NEHRP classification and based on Average Vs30 for all SH-SRT seismic sections and 1D Vs profiles over SRT-1. The estimation of seismic velocities (Vp and Vs) of a rock provides valuable information about the bulk physical properties of the rocks. This information does not only supply a great value during the design and construction phases, also may be cost-effective and non-destructive geotechnical site characterizations using seismic-wave methods.

Acknowledgements

We would like to express our immense gratitude to Dr. Fathi M. Abdullah from Taiz University for their valuable comments and discussions on an earlier version of the manuscript. We also show our gratitude to the Department of Applied Geology, University of Kirkuk, especially to Dr. Dhahir K. Ali. We would like to thank the two anonymous reviewers for their many insightful comments and suggestions.

Conflicts of Interest

The authors declare no conflict of interest.

References

- Abd El-Rahman, M., 1991 The potential of absorption coefficient and seismic quality factor in delineating less sound foundation materials in Jabal Shib Az Sahara area, Northwest of Sanaa, Yemen Arab Republic. *Egypt MERC Earth Sci*, 5, 181–187.
- Abd El-Rahman, M., 1989. Evaluation of the Kinetic Moduli of the surface material and application to engineering geologic map at Ma'Barr Sabah area (Dhamar province), Northern Yemen, Egypt. *J. Geol.*, 33, 229–250 .
- Abudeif, A. M., Abdel Aal, G. Z., Abdelbaky, N. F., Abdel Gowad, A. M., and Mohammed, M. A., 2023. Evaluation of Engineering Site and Subsurface Structures Using Seismic Refraction Tomography: A Case Study of Abydos Site, Sohag Governorate, Egypt. *Applied Sciences*, 13(4), 2745. <https://doi.org/10.3390/app13042745>
- Abudeif, A.; Mohammed, M.; Abd El-Aal, A.; Omar, K.A., 2019. Single and multi-channel passive source methods for calculating the shallow S-wave velocity structure and site effect parameters at 15th May City, Egypt. *J. Afr. Earth Sci.*, 159, 103579. <https://doi.org/10.1016/j.jafrearsci.2019.103579>
- Al-Gburi, H. F., Al-Tawash, B. S., Al-Tamimi, O. S. and Schüth, C., 2023. Impacts of hydrogeochemical processes and land use practices on groundwater quality of Shwan sub-Basin, Kirkuk, northern Iraq. *Heliyon*, 9(3). <https://doi.org/10.1016/j.heliyon.2023.e13995>
- Al-Heety, A. J., 2016. Velocities Extraction Efficiency of Shear Waves from Rayleigh Waves by Applying Multichannel Analysis of Surface Waves Technique and Their Relation by A Number of Geotechnical Parameters. *Iraqi Bulletin of Geology and Mining*, 12(2).1-10 (in Arabic)
- Al-Heety, A. J., 2018b. An Evaluation between Time-term, Reciprocal Time and Refraction Tomography Analysis Methods for obtaining 2-D shallow Seismic Velocity Models over Synthetic Traveltimes. <https://doi.org/10.31223/osf.io/gbqe6>
- Al-Heety, A. J., and Shanshal, Z. M., 2016. Integration of seismic refraction tomography and electrical resistivity tomography in engineering geophysics for soil characterization. *Arabian Journal of Geosciences*, 9, 1-11. <https://doi.org/10.1007/s12517-015-2116-9>
- Al-Heety, A. J., Al-Khalidy, A. A., and Al-Khafaji, A. J., 2016. Ground Penetrating Radar in Civil Engineering Application: Case Study of Multistorey Building Foundation Site to Mapping Subsurface Features at the Center of Karbala Governorate, Iraq. *The Iraqi Geological Journal*, 49-66. <https://doi.org/10.46717/igj.39-49.1.4Ms-2016-06-26>
- Al-Heety, A. J., Hassouneh, M. and Abdullah, F. M., 2021. Application of MASW and ERT methods for geotechnical site characterization: A case study for roads construction and infrastructure assessment in Abu Dhabi, UAE. *Journal of Applied Geophysics*, 193, 104408. <https://doi.org/10.1016/j.jappgeo.2021.104408>
- Al-Heety, A. J., Shanshal, Z. M., and Al-Mashhadany, A. Y., 2022. Application of Multi-Channel Analysis Surface Waves and Electrical Resistivity Tomography Methods to Identify Weak Zones at University of Mosul, Northern Iraq. *The Iraqi Geological Journal*, 47-69. <https://doi.org/10.46717/igj.55.1D.4Ms-2022-04-20>
- Ali, D. K., 2023. Self-Potential Investigation for Near-Surface Depression Delineation in Seikanian Kirkuk, Iraq. *The Iraqi Geological Journal*, 30-38. <https://doi.org/10.46717/igj.56.2D.3ms-2023-10-9>
- Al-Nuaiemy, A. Z., Al-Juraisy, B. A. and Al-Mafraji, M. A., 2018. The Use of the Seismic Refraction Tomography Survey Method and the Multi-Channel Analysis Technique of Surface Waves in the Geotechnical Assessment of the Al-Amal Apartments Site in Kirkuk, Northern Iraq, *Iraqi National Journal of Earth Science*, 18(2), 89-104. (In Arabic) <https://doi.org/10.33899/EARTH.2018.159260>.

- Al-Saigh, N. H. and Jaddoa Al-Heety A., 2014. Seismic refraction tomography and MASW survey for geotechnical evaluation of soil for the teaching hospital project at Mosul University. *Journal of Zankoy Sulaimani-Part A (JZS-A)*, 16(1), 1-14. <https://doi.org/10.17656/jzs.10279>
- Al-Saigh, N.H. and Al-Heety, A. J., 2018. 2-D Seismic Refraction Tomography for Site Investigation of the Teaching Hospital Project at Mosul University, 18 (1), 77-86. (In Arabic) <https://doi.org/10.33899/earth.2018.159280>
- Azwin, I. N., Saad, R. and Nordiana, M., 2013. Applying the seismic refraction tomography for site characterization. *APCBEE procedia*, 5, 227-231. <https://doi.org/10.1016/j.apcb.2013.05.039>
- Baban, E. N., Amin, A. K. and Mohammed, S. S., 2022. Seismic Refraction Tomography and Geotechnical Parameters to Assess the Chaqchaq Dam failure in NW Sulaimani City, Kurdistan Region, Iraq. *Iraqi National Journal of Earth Science*, 22(2), 121-139. <https://doi.org/10.33899/EARTH.2022.135251.1027>.
- Baban, E., Amin, A. and Ahmed, K., 2023. Combined Geoelectrical Tomography (ERT/IP) Methods and Geoelectrical Parameters to Evaluate Groundwater in Qularaisi Area NW Sulaimani-Kurdistan Region-IRAQ. *Iraqi National Journal of Earth Science*, 23(1), 1-34. <https://doi.org/10.33899/EARTH.2023.135144.1024>
- Bery, A. A., 2013. High resolution in seismic refraction tomography for environmental study, *International Journal of Geosciences* 4(04):792-796. <https://doi.org/10.4236/ijg.2013.44073>
- Bhowmick, S., 2017. Role of Vp/Vs and Poisson's ratio in the assessment of foundation (s) for important civil structure (s). *Geotechnical and Geological Engineering*, 35, 527-534. <https://doi.org/10.1007/s10706-016-0106-7>
- Bieniawski, Z.T., 1975 Point Load Test in Geotechnical Practice. *Engineering Geology*, 9, 1-11. [https://doi.org/10.1016/0013-7952\(75\)90024-1](https://doi.org/10.1016/0013-7952(75)90024-1)
- Bowles, J.E. *Foundation Analysis and Design*, 2nd ed.; McGraw-Hill International Book Company: London, UK, 1988; p. 587 .
- Butchibabu, B., Jha, P. C., Sandeep, N. and Sivaram, Y. V., 2023. Seismic refraction tomography using underwater and land based seismic data for evaluation of foundation of civil structures. *Journal of Applied Geophysics*, 210, 104934. <https://doi.org/10.1016/j.jappgeo.2023.104934>
- Cardarelli, E., Cercato, M. and De Donno, G., 2014. Characterization of an earth-filled dam through the combined use of electrical resistivity tomography, P-and SH-wave seismic tomography and surface wave data. *Journal of Applied Geophysics*, 106, 87-95. <https://doi.org/10.1016/j.jappgeo.2014.04.007>
- Das, S. K. and Basudhar, P. K., 2009. Utilization of self-organizing map and fuzzy clustering for site characterization using piezocone data. *Computers and Geotechnics*, 36(1-2), 241-248. <https://doi.org/10.1016/j.compgeo.2008.02.005>
- Donohue, S., Gavin, K. and Tolooiyan, A., 2011. Geophysical and geotechnical assessment of a railway embankment failure. *Near Surface Geophysics*, 9(1), 33-44. <https://doi.org/10.3997/1873-0604.2010040>
- Ehlers, C. J., Lobley, G., Spikula, D. R. and Brand, J. R., 2008. Site Characterization through the Integration of Geophysical and Geotechnical Data. In *Offshore Technology Conference* (pp. OTC-19349). OTC. <https://doi.org/10.4043/19349-MS>
- EL Hameedy, M. A., Mabrouk, W. M., Dahroug, S., Youssef, M. S. and Metwally, A. M., 2023. Role of Seismic Refraction Tomography (SRT) in bedrock mapping; case study from industrial zone, Ain-Sokhna area, Egypt. *Contributions to Geophysics and Geodesy*, 53(2), 111-128. <https://doi.org/10.31577/congeo.2023.53.2.2>

- El Sharawy, M.S., Nabawy, B.S., 2016. Determination of electrofacies using wireline logs based on multivariate statistical analysis for the Kareem Formation, Gulf of Suez, Egypt. *Environ. Earth Sci.*, 75, 1394. <https://doi.org/10.1007/s12665-016-6214-0>
- EN 1998-1: 2004; Eurocode 8: Design of Structures for Earthquake Resistance-Part 1: General Rules, Seismic Actions and Rules for Buildings. European Committee for Standardization: Brussels, Belgium, 2004.
- Fang, K., Zhao, T., Zhang, Y., Qiu, Y. and Zhou, J., 2019. Rock cone penetration test under lateral confining pressure. *International Journal of Rock Mechanics and Mining Sciences*, 119, 149-155. <https://doi.org/10.1016/j.ijrmms.2019.04.018>
- Foti, S., Parolai, S., Albarello, D. and Picozzi, M., 2011. Application of surface-wave methods for seismic site characterization. *Surveys in geophysics*, 32, 777-825. <https://doi.org/10.1007/s10712-011-9134-2>
- Gamal, M. and Hanafy, S., 2004. Assessment of seismic hazards and engineering problems at newly constructed cities in Egypt. SEG Technical Program Expanded Abstracts, pp.490-493 ,
- Gardi, S. Q. S., Al-Heety, A. J. R. and Mawlood, R. Z., 2015. 2D electrical resistivity tomography for the investigation of the subsurface structures at the Shaqlawa proposed dam site at Erbil Governorate, NE Iraq. *International Journal of Science and Research*, 4, 607-614.
- Gardi, S. Q. S., Al-Heety, A. J. and Mawlood, R. Z., 2018. Engineering site investigation using 2D Electrical Resistivity Tomography at the Siktan proposed Dam site at Erbil Governorate, Iraqi Kurdistan Region. *Journal of Duhok University*, 142-154. <https://doi.org/10.26682/sjuod.2018.20.1.13>.
- Gardner, G.; Gardner, L.; Gregory, A., 1974. Formation velocity and density—The diagnostic basics for stratigraphic traps. *Geophysics* , 39, 770–780 . <https://doi.org/10.1190/1.1440465>
- Geometrics SeisImager, 2009. SeisImager/2DTM Manual Version 3.3.
- Geometrics SeisImager, 2019. Windows software package for seismic refraction analysis, Ver. 5. Geometrics Inc .
- Hayashi, K., and Takahashi, T., 2001. High resolution seismic refraction method using surface and borehole data for site characterization of rocks. *International Journal of Rock Mechanics and Mining Sciences*, 38(6), 807-813. [https://doi.org/10.1016/S1365-1609\(01\)00045-4](https://doi.org/10.1016/S1365-1609(01)00045-4)
- Hiltunen, D. R., and Cramer, B. J., 2008. Application of seismic refraction tomography in karst terrane. *Journal of Geotechnical and Geoenvironmental Engineering*, 134(7), 938-948. [https://doi.org/10.1061/\(ASCE\)1090-0241\(2008\)134:7\(938\)](https://doi.org/10.1061/(ASCE)1090-0241(2008)134:7(938))
- Hunt, R. E., 2005. *Geotechnical engineering investigation handbook*. Crc Press.
- Hunter, J. A., Crow, H. L., Stephenson, W. J., Pugin, A. J. M., Williams, R. A., Harris, J. B. and Woolery, E. W., 2022. Seismic site characterization with shear wave (SH) reflection and refraction methods. *Journal of Seismology*, 26(4), 631-652. <https://doi.org/10.1007/s10950-021-10042-z>
- Imai, T.; Fumoto, H., Yokota, K., 1976. P-and S-Wave Velocities in Subsurface Layers of Ground in Japan; Urawa Research Inst., Oyo Corporation: Saitama, Japan.
- Jassim S.Z., Goff J.C., 2006. *Geology of Iraq*. 1st Edition Dolin, Prague and Moravian Museum, Brno, Czech Republic .
- Kanlı, A. I., 2009. Initial velocity model construction of seismic tomography in near-surface applications. *Journal of Applied Geophysics*, 67(1), 52-62. <https://doi.org/10.1016/j.jappgeo.2008.09.005>

- Kearey, P., Brooks, M. and Hill, I., 2002. An introduction to geophysical exploration (Vol. 4). John Wiley and Sons.
- Khalil, M. H. and Hanafy, S. M., 2016. Geotechnical parameters from seismic measurements: Two field examples from Egypt and Saudi Arabia. *Journal of Environmental and Engineering Geophysics*, 21(1), 13-28. <https://doi.org/10.2113/JEEG21.1.13>
- Metwally, A., Hanafy, S., Guo, B. and Kosmicki, M., 2017. Imaging of subsurface faults using refraction migration with fault flooding. *Journal of Applied Geophysics*, 143, 103-115. <https://doi.org/10.1016/j.jappgeo.2017.05.003>
- Miller, G. A., Tan, N. K., Collins, R. W. and Muraleetharan, K. K., 2018. Cone penetration testing in unsaturated soils. *Transportation Geotechnics*, 17, 85-99. <https://doi.org/10.1016/j.trgeo.2018.09.008>
- Mohamed, A. M., El Ata, A. A., Azim, F. A. and Taha, M. A., 2013. Site-specific shear wave velocity investigation for geotechnical engineering applications using seismic refraction and 2D multi-channel analysis of surface waves. *NRIAG Journal of Astronomy and Geophysics*, 2(1), 88-101. <https://doi.org/10.1016/j.nrjag.2013.06.012>
- Mohammed, M., Abudeif, A., Abd El-aal, A., 2020. Engineering geotechnical evaluation of soil for foundation purposes using shallow seismic refraction and MASW in 15th Mayo, Egypt. *J. Afr. Earth Sci.*, 162, 103721. <https://doi.org/10.1016/j.jafrearsci.2019.103721>
- Ozcep, F. and Ozcep, T., 2011. Geophysical analysis of the soils for civil (Geotechnical) engineering and urban planning purposes: Some case histories from Turkey. *Int. J. Phys. Sci*, 6, 1169-1195.
- Park, C. B., Miller, R. D. and Xia, J., 1999. Multichannel analysis of surface waves. *Geophysics*, 64(3), 800-808. <https://doi.org/10.1190/1.1444590>
- Park, C., Richter, J., Rodrigues, R. and Cirone, A., 2018. MASW applications for road construction and maintenance. *The Leading Edge*, 37(10), 724-730. <https://doi.org/10.1190/tle37100724.1>
- Pasquet, S., Sauvin, G., Andriamboavonjy, M. R., Bodet, L., Lecomte, I. and Guérin, R., 2014. "Surface-wave dispersion inversion versus SH wave refraction tomography in saturated and poorly dispersive quick clays." 20th European Meeting of Environmental and Engineering Geophysics, Athens and Houten, Netherlands. <https://doi.org/10.3997/2214-4609.20142045>
- Pegah, E. and Liu, H., 2016. Application of near-surface seismic refraction tomography and multichannel analysis of surface waves for geotechnical site characterizations: A case study. *Engineering Geology*, 208, 100-113. <https://doi.org/10.1016/j.enggeo.2016.04.021>
- Salem, H. S., 2000. Poisson's ratio and the porosity of surface soils and shallow sediments, determined from seismic compressional and shear wave velocities. *Geotechnique*, 50(4), 461-463. <https://doi.org/10.1680/geot.2000.50.4.461>
- Shakir, A. M., Foti, S., Garofalo, F., Hijab, B. R. and Laftah, A. A., 2013. Laterally constrained inversion of surface wave data at Najaf city (Iraq). *Soil Dynamics and Earthquake Engineering*, 45, 89-95. <https://doi.org/10.1016/j.soildyn.2012.11.003>
- Shazly, T. F., Khafeef, E., Abd El Hady, A., Saleh, S. S., Soleman, S. and Farag, M. H., 2023. Utilizing Shallow Seismic Refraction, Electric Resistivity Tomography, and Ground Penetrating Radar Techniques, to Evaluate Geotechnical Properties at El Galala Plateau, Gulf of Suez, Egypt. *Iraqi National Journal of Earth Science*, 23(2), 218-238. <https://doi.org/10.33899/EARTH.2023.139838.1076>

- Sheehan, J. R., Doll, W. E. and Mandell, W. A., 2005. An evaluation of methods and available software for seismic refraction tomography analysis. *Journal of Environmental and Engineering Geophysics*, 10(1), 21-34. <https://doi.org/10.2113/JEEG10.1.21>
- Sheriff, R. E., 2002. *Encyclopedic Dictionary of Applied Geophysics*. Tulsa, OK: SEG ,
- Sheriff, R. E. and Geldart, L. P., 1995. *Exploration seismology*. Cambridge university press, Cambridge, UK
- Shimobe, S. and Spagnoli, G., 2020. Fall cone tests considering water content, cone penetration index, and plasticity angle of fine-grained soils. *Journal of Rock Mechanics and Geotechnical Engineering*, 12(6), 1347-1355. <https://doi.org/10.1016/j.jrmge.2020.02.005>
- Sissakian, V.K. and Al-Jibouri, B.M., 2012. Stratigraphy of the Low Folded Zone. *Iraqi Bulletin of Geology and Mining*, Special Issue, No. 5, 63-132.
- Sitharam, T. G. and Anbazhagan, P., 2008. Seismic microzonation: principles, practices and experiments. *EJGE Special Volume Bouquet*, 8, 61.
- Stümpel, H.; Kähler, S., Meissner, R., Milkereit, B., 1984. The use of seismic shear waves and compressional waves for lithological problems of shallow sediments. *Geophys. Prospect.*, 32, 662–675 .<https://doi.org/10.1111/j.1365-2478.1984.tb01712.x>
- Toksoz, M.N., Cheng, C.H. and Timur, A., 1976. Velocities of seismic waves in porous rocks, *Geophysics*, 41, 621-645. <https://doi.org/10.1190/1.1440639>
- Uhlemann, S., Hagedorn, S., Dashwood, B., Maurer, H., Gunn, D., Dijkstra, T. and Chambers, J., 2016. Landslide characterization using P-and S-wave seismic refraction tomography—The importance of elastic moduli. *Journal of Applied Geophysics*, 134, 64-76. <https://doi.org/10.1016/j.jappgeo.2016.08.014>
- Watkins, J.S., Walters, L.A., Godson, R.H. Dependence of in-situ compressional-wave velocity on porosity in unsaturated rocks. *Geophysics* 1972, 37, 29–35. <https://doi.org/10.1190/1.1440249>
- Xia J., Miller R.D., Park C.B., Wightman E. and Nigbor R., 2002. A pitfall in shallow shear-wave refraction surveying, *Journal of Applied Geophysics*, vol. 51, issue 1, 1-9 pp. [https://doi.org/10.1016/S0926-9851\(02\)00197-0](https://doi.org/10.1016/S0926-9851(02)00197-0)
- Xia, J., Miller, R. D. and Park, C. B., 1999. Estimation of near-surface shear-wave velocity by inversion of Rayleigh waves. *Geophysics*, 64(3), 691-700. <https://doi.org/10.1190/1.1444578>
- Xia, J., Miller, R. D., Park, C. B. and Ivanov, J., 2000. Construction of 2-D vertical shear-wave velocity field by the multichannel analysis of surface wave technique. In *13th EEGS Symposium on the Application of Geophysics to Engineering and Environmental Problems* (pp. cp-200). EAGE. https://doi.org/10.3997/2214-4609-pdb.200.2000_135
- Zhang, J. and Toksöz, M. N., 1998. Nonlinear refraction travelttime tomography. *Geophysics*, 63(5), 1726-1737. <https://doi.org/10.1190/1.1444468> .